Journal of Sound and Vibration (2001) **244**(1), 1–19
doi:10.1006/jsvi.2000.3451, available online at http://www.idealibrary.com on IDEAL®

THE STRUCTURE OF WOBBLING SOUND FIELDS

M. CARLEY

Department of Mechanical Engineering, University of Bath, Bath BA2 7AY, England

(*Received* 6 *April* 2000, *and in final form* 29 *September* 2000)

The acoustic field of rotating sources such as aeroplane propellers and helicopter rotors is known to develop a marked asymmetry when the incoming flow is not parallel to the axis of rotation. This effect has been modelled using a field composed of "wobbling modes", azimuthal modes whose amplitude is a function of azimuth. A computationally efficient method is developed for the calculation of these wobbling modes and of the acoustic field at incidence. Results are presented for operating conditions representative of a range of aircraft from a high-speed propeller at low incidence to a helicopter rotor. Detailed contour plots of the acoustic pressure are presented and discussed in the context of the geometry of the acoustic field. The field structure is interpreted in terms of the tunnelling of acoustic radiation across a transition region around the sonic radius (where the source has a Mach number of unity) and the asymmetry of the field is shown to arise from variations in the thickness of this transition region as the sonic radius varies during a revolution of the rotor.

1. INTRODUCTION

The calculation of the acoustic field radiated by aeroplane propellers and helicopter rotors is a problem which is of interest for both technological and scientific reasons. As the environmental requirement for reduced exterior noise and the commercial demand for lower interior noise drive propulsion development, the need to be able to predict noise levels accurately at the design stage becomes more important. At present, the main trend in propeller design is the development of high-speed systems which operate in the transonic or supersonic regime. The prediction of noise from such designs is difficult both because of the complex aerodynamics involved and because of the difficulty of calculating the noise radiated by a source which may be moving supersonically. Similarly, helicopter rotors have very complex aerodynamics and, furthermore, demonstrate an extreme form of the problem studied in this paper, that of incidence. Assuming, however, that the aerodynamics of the rotor can be calculated, exact theories of aerodynamic noise generation exist [1–3] which can be used to calculate the radiated noise. The theories of noise generation by moving solid bodies have existed for about 30 years and have been recast into forms suitable for efficient numerical evaluation [4–6]. The accurate computation of propeller noise is thus commonplace in industry. With increased computing power and the development of methods suitable for implementation on parallel computers [7], the time required for calculation of noise directivities has been reduced. On the other hand, the understanding of the physics of the noise generation process has not advanced as quickly and, for this reason, a number of approximate methods have been developed.

Approximate methods of propeller noise prediction have existed in various forms, beginning with point source approaches [8–10], but they were typically developed because of the relative lack of available computing power and usually began from some *ad hoc*

0022-460X/01/260001 + 19 $35.00/0

approximation. More recently, methods have been developed which begin from an exact theory. These approaches, often based on asymptotic methods [11–13], give simple, accurate, closed-form equations for the radiated noise which can be used in design calculations and which also indicate explicitly the dependence of the noise on the propeller operating parameters. While these studies have usually aimed to provide methods suitable for industrial noise predictions, they have also been used to study the structure of the acoustic field of rotating sources in some detail, often making explicit connections with the theory of electromagnetic radiation [14].

A new development was the introduction of a method for the exact evaluation of the acoustic integrals in a model problem. This approach due to Chapman [15], reduced the two-dimensional integrals for the acoustic field of a stationary rotating source to one-dimensional integrals in a new co-ordinate system, allowing the acoustic field to be calculated quickly enough, and in enough detail, to allow its structure to be studied. This method has been extended to the case of a translating rotating source [16, 17] and this paper contains an extension to the problem of a source at incidence. It should be noted that throughout this paper, incidence is measured relative to the axial inflow condition so that a helicopter rotor is considered to be at approximately 90° incidence.

2. WOBBLING MODES

The problem of noise generated by propellers and rotors at incidence has been studied for about 30 years. It has long been known that a propeller at finite angle of attack has an acoustic field which is not symmetric about the axis of rotation, as in the axial inflow or non-translating case. This asymmetry is due to two effects, the first aerodynamic and the second acoustic. The aerodynamic effect, which was the first to be modelled [18], is due to the variation of blade incidence during a revolution. This causes the force on the blade to fluctuate as it rotates, and also alters the rate of momentum injection at the blade surface. This effect is quite well understood and its contribution to the acoustic field has been calculated for some 30 years.

The second effect, which is of interest in this paper, has been studied more recently. As a blade rotates, its radiation efficiency varies with azimuth so that the steady-source radiation is also affected by the angle of attack. This purely acoustic effect was initially studied by Stuff [19] and later by Mani [20], Hanson and Parzych [21], Envia [22] and Hanson [23]. With the exception of reference [21], these studies were analytical and aimed at understanding the physics of the acoustic process as well as providing prediction methods.

The work of Stuff [19] used nearfield and farfield point-force approximations to estimate the effect of crossflow on the acoustic field of a rotating source. It can thus be considered an extension of the earlier work of Gutin [9] or of Lowson [24]. The next advance in the area was that of Mani [20], who calculated, to first order in crossflow Mach number, the effect of incidence on the steady loading field and demonstrated good agreement with the experimental data. He concluded that the effect of asymmetric convection on the steady loading noise of high tip-speed, highly loaded propellers (i.e. most modern designs) may be much greater than the effect of unsteady loading—the effect of incidence may be unrelated to loading fluctuations. Hanson [23] developed this idea further and calculated the farfield steady loading noise without limit on the angle of attack. This work introduced the concept of the "wobbling mode". The acoustic field radiated by an azimuthal mode of the source is made up of azimuthal modes whose amplitude varies with angle. Since they can no longer be considered "spinning modes" as in the axial inflow case, they are said to wobble during

a revolution. The acoustic effect of incidence was explained by the variation of the Mach number of the source towards a field point, causing the Doppler factor in the acoustic integrals to vary. In related work [22], Envia concentrated on the problem of noise from a large-blade number propeller in high-speed flight. Under these conditions, the angle of attack is small (less than 5°) and using this approximation, acoustic expressions were derived which are valid in both the near and far field.

For the industrial prediction of noise from propellers at incidence, a number of methods exist. These can either incorporate explicitly the effect of a mean flow in the time [25] or frequency domain [21] or can account for it implicitly via the observer motion, as in many time domain formulations [4, 5]. A series of tests comparing predictions with data from NASA's Propeller Test Assessment aircraft have been conducted [26, 27] using time and frequency domain techniques respectively. The agreement in both cases was good, demonstrating the power of the prediction methods.

The *status quo* in studying noise from propellers at incidence is that there are methods which are exact but computationally intensive [21, 25] and methods which are quicker but limited to the far field [23] or to small angles of attack [20, 22]. It seems worthwhile then to develop an analysis which will allow the acoustic field to be calculated exactly, without restriction on incidence or observer position, to allow the physics of the radiation process to be studied. Such a method exists for propellers in forward flight [15–17] and in this paper it will be extended to propellers at incidence.

2.1 THE STRUCTURE OF ROTATING SOUND FIELDS

The framework for the analysis which follows is the method originally introduced by Chapman [15] as a model problem for rotor acoustics and later extended by Carley [16, 17] to cover propellers in forward flight and more general source distributions. Using these methods, it is possible to calculate the acoustic field of a rotor at a resolution of less than one wavelength, in a reasonable time. This allows the structure of the field to be studied. In particular, the far field, near field and the transition between them can be examined. Summarizing briefly, the main conclusion of these studies is that the field is divided by the sonic radius, the radius at which the rotating source has, or would have, a Mach number of unity. Around this radius, over a distance of about half an acoustic wavelength, the transition from the near to the far field occurs. When the rotor is subsonic, it lies completely within this region and the acoustic radiation must "tunnel" into the far field, emerging as quite weak sound. When the rotor lies partly outside this radius, it can radiate directly into the far field and the strong beaming pattern characteristic of supersonic rotors is observed. When the rotor is supersonic but does not extend beyond the transition region, the acoustic field is closer to that of a subsonic rotor, some energy still being lost in tunnelling.

With this in mind, there is another way of thinking about the effect of incidence on a rotor. At incidence, the sonic radius becomes a function of azimuth in the rotor plane (equation (23)). One can then think, for example, of a rotor which passes in and out of the far field as it rotates, causing asymmetry in the acoustic field. Such an effect will indeed be obvious in the results of section 4.

3. ACOUSTIC CALCULATIONS

The basic problem is illustrated in Figure 1. A propeller operates in a flow of vector Mach number $\mathbf{M}_\infty$. Co-ordinates are chosen so that the propeller axis lies along the z-axis of the

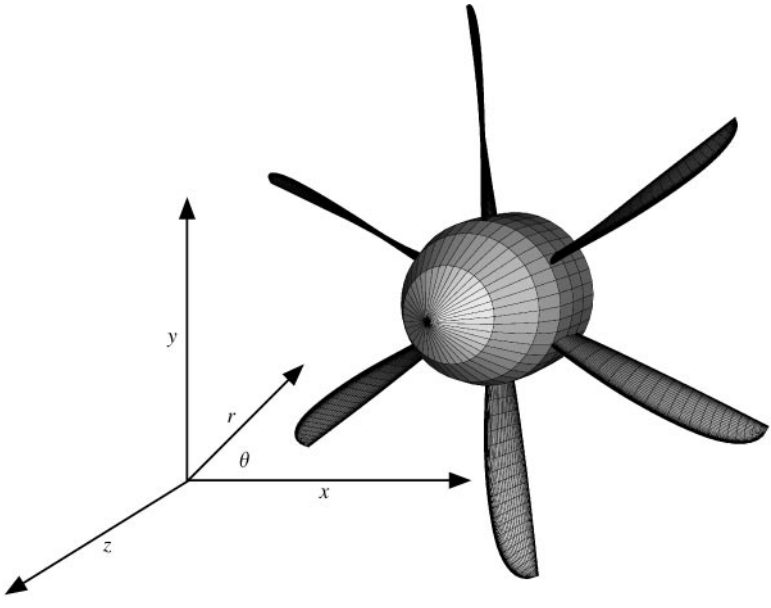

Figure 1. Co-ordinates for propeller and observer.

reference frame. Cylindrical co-ordinates (r, θ, z) are defined, with points on the propeller disc given by $(r_1, \theta_1, 0)$. The acoustic integrals are those of Goldstein [3] which, neglecting non-linear terms, are

$$p = \frac{\mathrm{D}}{\mathrm{D}t} \int_{-\infty}^{\infty} \int_{A(\tau)} G(\mathbf{x}, t; \mathbf{y}, \tau)\, \rho_0 v_n \, \mathrm{d}A \, \mathrm{d}\tau \quad \text{(thickness)}, \tag{1a}$$

$$-\nabla \cdot \int_{-\infty}^{\infty} \int_{A(\tau)} G(\mathbf{x}, t; \mathbf{y}, \tau)\, \mathbf{f}(r_1) \, \mathrm{d}A \, \mathrm{d}\tau \quad \text{(loading)}, \tag{1b}$$

where A is the surface of the source, ρ_0 is the unperturbed fluid density, v_n the fluid normal velocity at the source surface, $\mathbf{f}$ the force exerted on the fluid by the surface and the convective derivative $\mathrm{D}/\mathrm{D}t$ is defined as

$$\frac{\mathrm{D}}{\mathrm{D}t} = \frac{\partial}{\partial t} + c\mathbf{M}_\infty \cdot \nabla,$$

where c is the speed of sound in the fluid. Since the source due to the rotation of the blade geometry $h(r_1, \theta_1)$ is periodic it can be decomposed into a Fourier series in time and azimuth:

$$h = \sum_{n=-\infty}^{\infty} h_n \mathrm{e}^{-\mathrm{j}n(\Omega t + \theta_1)},$$

$$h_n(r_1) = \frac{1}{2\pi} \int_0^{2\pi} \mathrm{e}^{\mathrm{j}n\theta_1} h(r_1, \theta_1) \, \mathrm{d}\theta_1$$

and the nth component of the velocity perturbation, found by differentiating h, will be $-\mathrm{j}n\Omega h_n$.

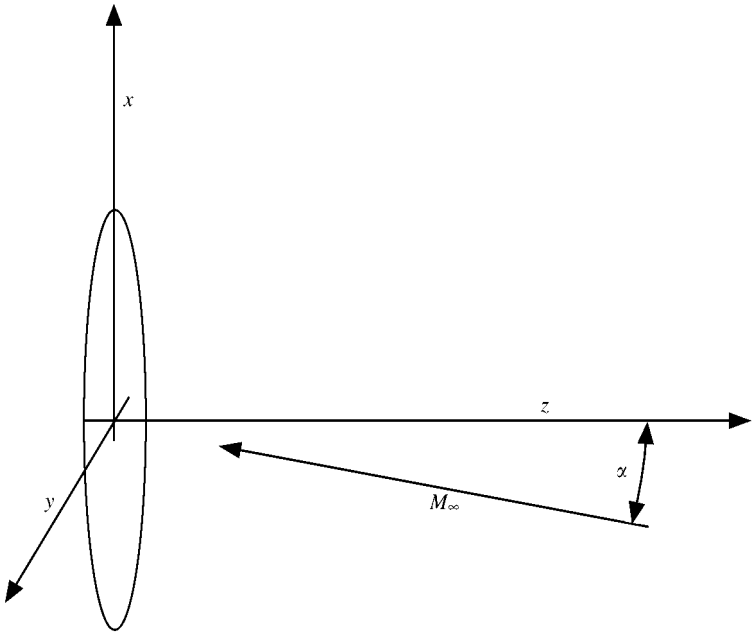

Figure 2. Co-ordinate system for inflow.

The Green's function G to be inserted into the acoustic integrals is that given by Garrick and Watkins [10],

$$G(\mathbf{x}, t; \mathbf{y}, \tau) = \frac{\delta(t - \tau - \sigma/c)}{4\pi S},$$

which in the frequency domain, for a source with time dependence $\exp -j\omega t$, is

$$G(\mathbf{x}, \mathbf{y}, \omega) = \frac{e^{jk\sigma}}{4\pi S}, \tag{2}$$

where $k = \omega/\beta^2 c$ (i.e. the acoustic wavenumber has been scaled on β^2 for convenience in later calculations) and the phase and amplitude radii σ and S, respectively, are given by

$$S = (\beta^2 |\mathbf{x} - \mathbf{y}|^2 + [\mathbf{M}_\infty \cdot (\mathbf{x} - \mathbf{y})]^2)^{1/2}, \tag{3a}$$

$$\sigma = S - \mathbf{M}_\infty \cdot (\mathbf{x} - \mathbf{y}), \tag{3b}$$

$$\beta = (1 - |\mathbf{M}_\infty|^2)^{1/2}.$$

Co-ordinates are chosen so that $\mathbf{M}_\infty = M_\infty(\sin\alpha, 0, -\cos\alpha) = (M_x, 0, -M_z)$ where α is the angle of incidence, i.e. the inflow is defined such that it corresponds to forward flight in the z direction, (Figure 2). Converting to cylindrical co-ordinates:

$$\mathbf{M}_\infty \cdot (\mathbf{x} - \mathbf{y}) = M_x(r\cos\theta - r_1\cos\theta_1) - M_z z. \tag{4}$$

At this point, the problem is simplified by assuming that source terms are independent of source radius r_1. It has been shown in a previous paper [17] how the results of the type of analysis which follows can be used to calculate the field from a source of arbitrary radial

dependence so this does not imply any loss of generality. The reason for the simplification is that it makes possible the evaluation of the acoustic integrals by an efficient numerical method. With this assumption, inserting the Green function into equation (1) and transforming θ_1 to $\theta_1 + \theta$, the acoustic integrals become

$$p_T = -\mathrm{j}nM_t(-\mathrm{j}nM_t + M_\infty \cdot \nabla) I(r, \theta, z), \tag{5a}$$

$$p_L = -\nabla \cdot I, \tag{5b}$$

$$I = \mathrm{e}^{-\mathrm{j}n\theta} \int_0^1 \int_0^{2\pi} \frac{\mathrm{e}^{\mathrm{j}(k\sigma - n\theta_1)}}{4\pi S} r_1 \, \mathrm{d}\theta_1 \, \mathrm{d}r_1, \tag{5c}$$

$$\mathbf{M}_\infty \cdot \nabla = M_x \frac{\partial}{\partial x} - M_z \frac{\partial}{\partial z},$$

$$= M_x \left(\cos\theta \frac{\partial}{\partial r} - \sin\theta \frac{1}{r} \frac{\partial}{\partial \theta} \right) - M_z \frac{\partial}{\partial z},$$

where lengths have been non-dimensionalized on rotor radius a, velocities on the speed of sound c and pressures on $\rho_0 c^2$. The tip Mach number $M_t = \Omega a/c$ and the wavenumber $k = nM_t/\beta^2$. With the transformation of θ_1,

$$S = (\beta^2 [r^2 + r_1^2 - 2rr_1 \cos\theta_1 + z^2] + [M_x(r\cos\theta - r_1\cos(\theta + \theta_1)) - M_z z]^2)^{1/2},$$

$$\sigma = S - M_x(r\cos\theta - r_1\cos(\theta + \theta_1)) + M_z z.$$

When the inflow is purely axial, I depends sinusoidally on θ and need only be calculated at each value of r and z. With the introduction of a crossflow M_x, if I is to be known exactly over the acoustic field, it must be calculated at every value of r, z and θ which may be of interest. The approximate methods described in section 2 can be used to reduce the effort involved but since an exact solution is required, a different approach will be used.

3.1 CALCULATION METHOD

The first step in the evaluation of I is the introduction of a co-ordinate transformation as in Chapman [15] (also reference [28], p. 227). The co-ordinate transformation is shown in Figure 3. The new co-ordinates (r_2, θ_2) are centred on the intersection of the observer sideline with the source plane, z remaining unchanged. With this transformation,

$$\mathbf{M}_\infty \cdot (\mathbf{x} - \mathbf{y}) = M_x[r\cos\theta - r_1\cos(\theta + \theta_1)] - M_z z$$

$$= -M_x r_2 \cos(\theta + \theta_2) - M_z z \tag{6}$$

and I is transformed to

$$I = \mathrm{e}^{-\mathrm{j}n\theta} \int_{max(0, r-1)}^{r+1} \int_{\theta_2^{(0)}}^{2\pi - \theta_2^{(0)}} \frac{\mathrm{e}^{\mathrm{j}(k\sigma - n\theta_1)}}{4\pi S} r_2 \, \mathrm{d}\theta_2 \, \mathrm{d}r_2, \tag{7}$$

$$S = [\beta^2 R^2 + (M_x r_2 \cos(\theta + \theta_2) + M_z z)^2]^{1/2},$$

$$\sigma = S + M_x r_2 \cos(\theta + \theta_2) + M_z z,$$

$$R^2 = r_2^2 + z^2.$$

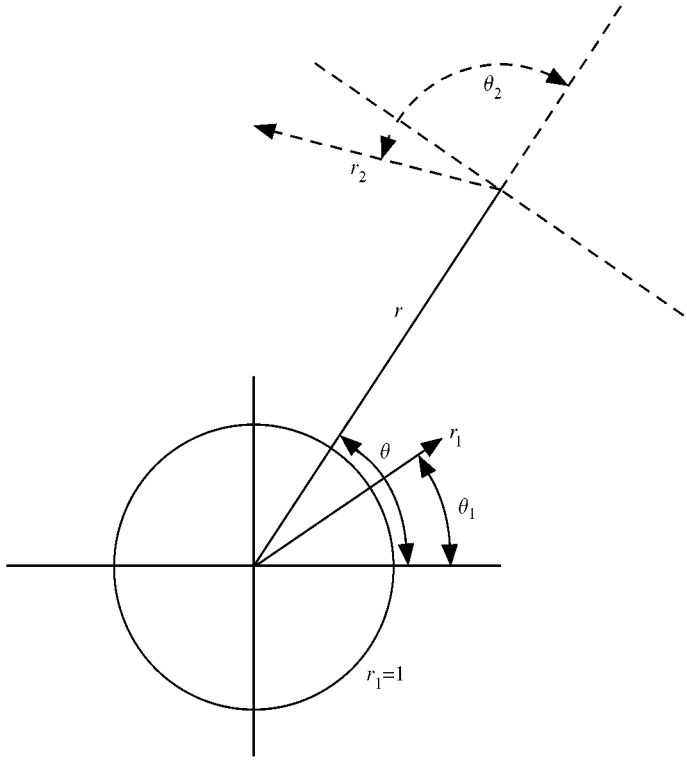

Figure 3. New co-ordinate system for acoustic integrals.

The limits on θ_2 are found from the intersection of a circle of radius r_2 centred on the observer sideline with the edge of the source disc $r_1 = 1$:

$$\theta_2^{(0)} = \cos^{-1}\frac{1 - r^2 - r_2^2}{2rr_2}.$$

This transformation has been used previously [15–17] in the calculation of the acoustic field of a rotor at zero incidence but to apply it to the incidence problem requires that the Green's function be expanded into a Fourier series in θ_2.

3.2. GREEN'S FUNCTION MODAL EXPANSION

The first stage in expanding the Green function is to apply the Bessel function addition theorem [29, 30]:

$$G = \frac{\mathrm{e}^{\mathrm{j}k(S + M_x r_2 \cos(\theta + \theta_2) + M_z z)}}{4\pi S},$$

$$= \frac{\mathrm{e}^{\mathrm{j}k(S + M_z z)}}{4\pi S} \sum_{m=-\infty}^{\infty} \mathrm{j}^m \mathrm{J}_m(kM_x r_2)\mathrm{e}^{\mathrm{j}m(\theta + \theta_2)}.$$

Then, assuming that $\exp[\mathrm{j}k(S-S_0)]S_0/S$ can be expanded in a Fourier series in θ_2,

$$G = \frac{\mathrm{e}^{\mathrm{j}k(S_0+M_z z)}}{4\pi S_0}\sum_{p=-\infty}^{\infty} g_p(r,r_2,z,k)\,\mathrm{e}^{\mathrm{j}p(\theta+\theta_2)}\sum_{m=-\infty}^{\infty}\mathrm{j}^m \mathrm{J}_m(kM_x r_2)\,\mathrm{e}^{\mathrm{j}m(\theta+\theta_2)},$$

$$\simeq \frac{\mathrm{e}^{\mathrm{j}k(S_0+M_z z)}}{4\pi S_0}\sum_{p=-P}^{P}\sum_{m=-M}^{M}\mathrm{j}^m g_p J_m(kM_x r_2)\,\mathrm{e}^{\mathrm{j}m\theta}\mathrm{e}^{\mathrm{j}(p+m)\theta_2}, \tag{8}$$

where g_p is the coefficient of $\exp \mathrm{j}p\theta_2$ in the Fourier series of $\exp \mathrm{j}k(S-S_0)S_0/S$ and S_0 is S evaluated at $\cos(\theta+\theta_2)=0$. For computational purposes, the Fourier expansion is restricted to $(2P+1)\times(2M+1)$ terms.

The calculation of the coefficients of the Fourier modes, g_p, starts from an expansion of G in powers of $\cos(\theta+\theta_2)$. The method adopted appears to be new although it has an obvious affinity with the techniques described by Van Dyke [31]. Beginning with Leibniz' rule for differentiation of a product [30], the uth derivative of $\exp[\mathrm{j}k(S-S_0)]S_0/S$ is written as

$$\frac{\mathrm{d}^u}{\mathrm{d}C^u}\left(\mathrm{e}^{\mathrm{j}k(S-S_0)}\frac{S_0}{S}\right) = \sum_{v=0}^{u}\binom{u}{v}\frac{\mathrm{d}^u}{\mathrm{d}C^u}\left(\mathrm{e}^{\mathrm{j}k(S-S_0)}\right)\frac{\mathrm{d}^{u-v}}{\mathrm{d}C^{u-v}}\left(\frac{S_0}{S}\right), \tag{9}$$

$$C = \cos(\theta+\theta_2).$$

The derivatives of S_0/S can be written directly from the power-series expansion of S^{-1}:

$$S^{-1} = [\beta^2 R^2 + (M_x r_2 C + M_z z)^2]^{-1/2},$$

$$= S_0^{-1}\left(1+\frac{\mathrm{j}M_x r_2 C}{\beta R+\mathrm{j}M_z z}\right)^{-1/2}\left(1-\frac{\mathrm{j}M_x r_2 C}{\beta R-\mathrm{j}M_z z}\right)^{-1/2},$$

$$= \frac{1}{S_0}\sum_{u=0}^{\infty} a_u\left(\frac{\mathrm{j}M_x r_2 C}{\beta R+\mathrm{j}M_z z}\right)^u \sum_{v=0}^{\infty} a_v\left(-\frac{\mathrm{j}M_x r_2 C}{\beta R-\mathrm{j}M_z z}\right)^v,$$

where a_u is the coefficient of x^u in the power-series expansion of $(1+x)^{-1/2}$. Noting that

$$\frac{\mathrm{j}M_x r_2 C}{\beta R+\mathrm{j}M_z z} = \mathrm{j}\frac{M_x r_2 C}{S_0}\mathrm{e}^{-\mathrm{j}\phi},$$

where

$$\phi = \tan^{-1}\frac{M_z z}{\beta R},$$

the summation can be rewritten as

$$\frac{1}{S} = \frac{1}{S_0}\sum_{u=0}^{\infty}\sum_{v=0}^{u} a_v a_{u-v}\left(\mathrm{j}\frac{M_x r_2 C}{S_0}\mathrm{e}^{-\mathrm{j}\phi}\right)^v\left(-\mathrm{j}\frac{M_x r_2 C}{S_0}\mathrm{e}^{\mathrm{j}\phi}\right)^{u-v}.$$

Rearranging the second summation to eliminate the complex terms, the summation reduces to

$$\frac{S_0}{S} = \sum_{u=0}^{\infty}\left(-\frac{M_x r_2\cos(\theta+\theta_2)}{S_0}\right)^u\sum_{v=0}^{u} a_v a_{u-v}\cos[(2v-u)(\phi+\pi/2)]$$

and the uth derivative of S_0/S with respect to $\cos(\theta + \theta_2)$, evaluated at $\cos(\theta + \theta_2) = 0$, is then

$$u!\left(-\frac{M_x r_2}{S_0}\right)^u \sum_{v=0}^{u} a_v a_{u-v} \cos[(2v-u)(\phi + \pi/2)]. \tag{10}$$

The derivatives of $\exp jk(S - S_0)$ are also needed and can be evaluated using a recursion relation. Starting with

$$\frac{\mathrm{d}}{\mathrm{d}C} \mathrm{e}^{\,jk(S-S_0)} = jk \frac{\mathrm{d}S}{\mathrm{d}C} \mathrm{e}^{\,jk(S-S_0)}$$

and then

$$\frac{\mathrm{d}^u}{\mathrm{d}C^u} \mathrm{e}^{\,jk(S-S_0)} = jk \sum_{v=0}^{u-1} \binom{u-1}{v} \frac{\mathrm{d}^{u-v-1}S}{\mathrm{d}C^{u-v-1}} \frac{\mathrm{d}^u}{\mathrm{d}C^u} \mathrm{e}^{\,jk(S-S_0)}, \tag{11}$$

the uth derivative of $\exp jk(S - S_0)$ can be evaluated using the derivatives of S and the lower order derivatives of $\exp jk(S - S_0)$. The derivatives of S, in turn, can be calculated by the following method:

$$S^2 = \beta^2 R^2 + (M_x r_2 C + M_z z)^2,$$

$$S\frac{\mathrm{d}S}{\mathrm{d}C} = M_x r_2 (M_x r_2 C + M_z z),$$

$$\left(\frac{\mathrm{d}S}{\mathrm{d}C}\right)^2 + S\frac{\mathrm{d}^2 S}{\mathrm{d}C^2} = M_x^2 r_2^2,$$

$$\frac{\mathrm{d}^u S^2}{\mathrm{d}C^u} = \sum_{v=0}^{u} \binom{u}{v} \frac{\mathrm{d}^v S}{\mathrm{d}C^v} \frac{\mathrm{d}^{u-v} S}{\mathrm{d}C^{u-v}} = 0, \quad u \geqslant 3,$$

so that

$$\frac{\mathrm{d}^u S}{\mathrm{d}C^u} = -\frac{1}{2S} \sum_{v=1}^{u-1} \binom{u}{v} \frac{\mathrm{d}^v S}{\mathrm{d}C^v} \frac{\mathrm{d}^{u-v} S}{\mathrm{d}C^{u-v}}, \quad u \geqslant 3. \tag{12}$$

The derivatives of $\exp jk(S - S_0)$ at $C = 0$ can then be evaluated using a recursion seeded with

$$S_0 = S|_{C=0} = [\beta^2 R^2 + M_z^2 z^2]^{1/2},$$

$$\left.\frac{\mathrm{d}S}{\mathrm{d}C}\right|_{C=0} = \frac{M_x M_z r_2 z}{S_0},$$

$$\left.\frac{\mathrm{d}^2 S}{\mathrm{d}C^2}\right|_{C=0} = \frac{M_x^2 r_2^2}{S_0} - \frac{1}{S_0}\left(\left.\frac{\mathrm{d}S}{\mathrm{d}C}\right|_{C=0}\right)^2,$$

$$\mathrm{e}^{jk(S-S_0)} = 1,$$

combined with equation (9) for the higher derivatives and equation (10) for the derivatives of $1/S$.

3.2.1. *Evaluation of modal coefficients*

Given the power-series expansion of the Green function, whose coefficients can be calculated exactly to arbitrary order, the evaluation of the modal coefficients is quite simple. The Green's function is represented by a Fourier series in θ_2:

$$\frac{e^{jkS}}{4\pi S} = \frac{e^{jkS_0}}{4\pi S_0} \sum_{p=-\infty}^{\infty} g_p e^{jp\theta_2}.$$

The coefficients g_p can be evaluated by direct integration of the power series,

$$g_p = \frac{S_0}{2\pi} \int_0^{2\pi} \frac{e^{jk(S-S_0)}}{S} e^{-jp\theta_2} d\theta_2,$$

$$= \sum_{m=0}^{\infty} \frac{G_m}{2\pi} \int_0^{2\pi} \cos^m(\theta + \theta_2) e^{-jp\theta_2} d\theta_2,$$

where G_m is the mth derivative of $\exp[jk(S-S_0)]S_0/S$ evaluated at $\cos(\theta+\theta_2)=0$, calculated numerically using the method described above. The integral in θ_2 is readily evaluated by the change of variables $\mu = \exp j\theta_2$:

$$\frac{1}{2\pi} \int_0^{2\pi} \cos^m(\theta+\theta_2) e^{-j\theta_2} d\theta_2 = \frac{1}{j2\pi} \oint_{|\mu|=1} (e^{j\theta}\mu + e^{-j\theta}/\mu)^m \frac{1}{\mu^{p+1}} d\mu,$$

$$= \frac{1}{2^m} \sum_{q}^{m} \binom{m}{q} \frac{e^{j(2q-m)\theta}}{j2\pi} \oint_{|\mu|=1} \mu^{2q-m-p-1} d\mu.$$

Evaluating the integrals in terms of their residues at the poles, only terms with $2q - m - p = 0$ contribute and the resulting modal coefficient is

$$g_p = e^{jp\theta} \sum_{m=0}^{\infty} \binom{p+2m}{p+m} \frac{G_{p+2m}}{2^{2p+2m}}. \tag{13}$$

3.3. EVALUATION OF I

Given the coefficients g_p, the acoustic integral I can be written

$$I = \int_{max(0,\, r-1)}^{r+1} \int_{\theta_2^{(0)}}^{2\pi-\theta_2^{(0)}} \frac{e^{j(k\sigma - n\theta_1)}}{4\pi S} r_2 \, d\theta_2 \, dr_2, \tag{14}$$

$$= \frac{1}{2} \sum_{p=-P}^{P} \sum_{m=-M}^{M} j^m e^{j(p+m)\theta}$$

$$\times \int_{max(0,\, r-1)}^{r+1} e^{jk(S_0 + M_z z)} g_p J_m(kM_x r_2) K_{n,m+p} r_2 \, dr_2, \tag{15}$$

$$K_{n,m+p}(r, r_2) = \frac{1}{2\pi} \int_{\theta_2^{(0)}}^{2\pi-\theta_2^{(0)}} e^{j[(p+m)\theta_2 - n\theta_1]} d\theta_2. \tag{16}$$

The function K can be evaluated analytically in closed form and this allows the efficient, exact, evaluation of I. From this point on, it will be assumed that n is even, $n = 2u$. The odd mode case can, however, be handled by similar methods to those used here [16]. It is worth noting at this point that the integrals of equation (15) are integrals over the source disc where the integrand has angular variation $\exp j[(p+m)-n]\theta_1$. This is equivalent to calculating the field due to a fluctuating rotating source [18], but where the unsteadiness is due purely to asymmetric propagation. It should also be noted that the "equivalent unsteady source" depends on the observer position, the coefficients g_p being functions of the observer co-ordinates.

The integral definition of K, equation (16), is first rewritten as a complex integral using the relations (Figure 3),

$$r_1 e^{-j\theta_1} = \frac{r}{\mu}(\mu + t),$$

$$r_1^2 = r^2 \frac{t}{\mu}(\mu + \eta)(\mu + t),$$

where $t = r_2/r$ and $\eta = r/r_2$ and the contour of integration is part of the unit circle. The definition of $K_{2u,v}$ can then be written as

$$K_{2u,v}(r, r_2) = \frac{t^{-u}}{j2\pi} \int_{\mu_o}^{\mu_o^*} \frac{(\mu + t)^u}{(\mu + \eta)^u} \frac{\mu^v}{\mu^{u+1}} \, d\mu, \tag{17}$$

which can be expanded to

$$K_{2u,v}(r, r_2) = \sum_{q=0}^{u} \binom{u}{q} t^{-q} \psi_{u,v+q-u-1}(r, r_2),$$

where $\psi_{u,s}$ is defined as

$$\psi_{u,s}(r, r_2) = \frac{1}{j2\pi} \int_{\mu_o}^{\mu_o^*} \frac{\mu^s}{(\mu + \eta)^u} \, d\mu. \tag{18}$$

The function $\psi_{u,s}$ is calculated in closed form using different methods depending on the values of u and s. When $s < 0$, the integrand is expanded into partial fractions [32]:

$$\frac{1}{(\mu + \eta)^u} \frac{1}{\mu^{-s}} = \sum_{i=1}^{-s} \frac{A_i}{\mu^i} + \sum_{i=1}^{u} \frac{B_i}{(\mu + \eta)^i},$$

$$A_i = \frac{1}{(-s-i)!} \frac{d^{-s-i}}{d\mu^{-s-i}} \frac{1}{(\mu + \eta)^u}\bigg|_{\mu=0},$$

$$= (-)^{-s-i} t^{u+s-i} \binom{u-s-i-1}{s-i},$$

$$B_i = \frac{1}{(u-i)!} \frac{d^{u-i}}{d\mu^{-s-i}} \frac{1}{\mu^{-s}}\bigg|_{\mu=-\eta},$$

$$= (-)^{-s} t^{u-s-i} \binom{u-s-i-1}{-s-1},$$

so that

$$\psi_{u,s} = -\frac{(-)^s}{\pi}\sum_{i=1}^{u}\binom{u-s-i-1}{u-1}t^{u-s-i}\frac{r_2^{i-1}\sin(i-1)\alpha}{i-1}$$
$$-\frac{(-)^s}{\pi}\sum_{i=1}^{-s}(-)^i\binom{u-s-i-1}{-s-1}t^{u-s-i}\frac{\sin(i-1)\theta_2^{(0)}}{i-1}, \quad s<0. \quad (19)$$

where

$$\alpha = \tan^{-1}\frac{\sin\theta_2^{(0)}}{\eta+\cos\theta_2^{(0)}},$$

and for $i=1$ in the summations

$$\frac{\sin(1-i)\theta_2^{(0)}}{1-i} \text{ is replaced by } \theta_2^{(0)}-\pi$$

and

$$\frac{\sin(1-i)\alpha}{1-i} \text{ is replaced by}$$

$$\alpha, \quad t\leqslant 1,$$

$$\alpha-\pi, \quad t>1.$$

When $0\leqslant s<u-1$, successive application of the identity [30, 2.111.2]

$$\int\frac{x^n}{(a+bx)^m}\,dx = \frac{x^n}{(a+bx)^{m-1}(n+1-m)b} - \frac{na}{(n+1-m)b}\int\frac{x^{n-1}}{(a+bx)^m}\,dx,$$

or integration by parts, yields

$$\psi_{u,s} = \frac{r_2^{u-1}}{\pi}\sum_{i=0}^{s}(-\eta)^i\frac{s!}{(s-i)!}\frac{\sin[(u-1)\alpha-(s-i)\theta_2^{(0)}]}{(s+1-u-i)\cdots(s+1-u)}. \quad (20)$$

When $s\geqslant u-1$, this identity can only be applied $s-u$ times and the formula [30, 2.111.3]

$$\int\frac{x^{m-1}}{(a+bx)^m}\,dx = -\frac{x^{m-1}}{(a+bx)^{m-1}(m-1)b} + \frac{1}{(m-1)b}\int\frac{x^{m-2}}{(a+bx)^{m-1}}\,dx,$$

must be used to give

$$\psi_{u,s} = \frac{r_2^{u-1}}{\pi}\sum_{i=0}^{s-u}(-\eta)^i\frac{s!}{(s-i)!}\frac{\sin[(u-1)\alpha-(s-i)\theta_2^{(0)}]}{(s+1-u-i)\cdots(s+1-u)}$$
$$-\frac{1}{\pi}\frac{s!}{u!}\frac{(-\eta)^{s-u+1}}{(s+1-u)!}\sum_{i=1}^{u}\frac{r_2^{u-i}\sin[(u-i)(\alpha-\theta_2^{(0)})]}{u-i}. \quad (21)$$

The contour of integration of equation (18) depends on the relative values of r and r_2, as shown in Figure 4. As r_2 varies, the limits on θ_2 also change, thus altering the contour of

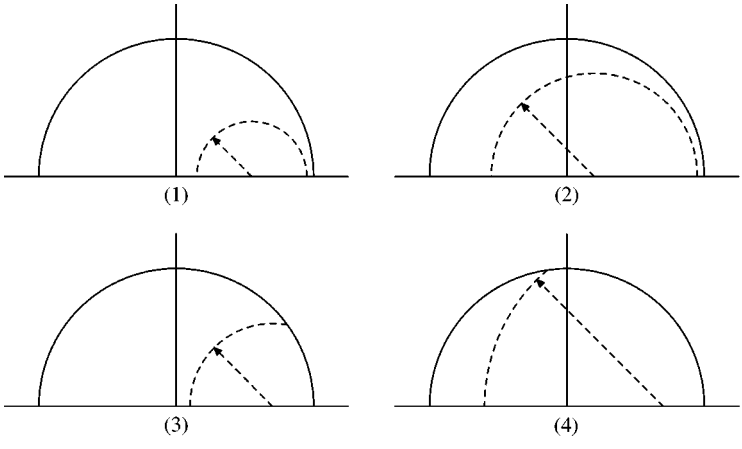

Figure 4. Different cases for determination of limits in integral representation of $\psi_{u,s}$ in equation (18). The limits are determined by the intersection of a circle of radius r_2 (shown dashed) with a circle of radius $r_1 = 1$. (1) $r > 1/2$, $r_2 < 1 - r$; (2) $r < 1/2$, $r < r_2 < 1 - r$; (3) $r > 1/2$, $1 - r < r_2 < r$; (4) $r_2 > r$.

integration. In cases 1 and 2 of Figure 4, where $r < 1$ and $r_2 < 1 - r$, the contour of integration in equation (18) is closed and the integral can be evaluated using Cauchy's residue theorem. For $s < 0$, $\psi_{u,s}$ depends only on the residues at the singularities enclosed by the contour, these singularities being at 0 and $-\eta$. In case 1, $r < 1/2$ and $r < r_2 < 1 - r$, both singularities are enclosed and, since $A_1 \equiv -B_1$, $\psi_{u,s} \equiv 0$. In case 2, $1/2 < r < 1$, $r_2 < 1 - r$,

$$\psi_{u,s} = -(-)^s t^{u-s-1} \binom{u-s-2}{-s-1}.$$

When $s > 0$, there is only one singularity, that at $-\eta$. When this singularity is enclosed, $\psi_{u,s} = (-\eta)^s$ and $\psi_{u,s} \equiv 0$ otherwise, for $u > 1$.

3.3.1. *Infinite series expansions*

Finally, infinite series expansions are also needed for the calculation of K. When r is small (i.e., for observer positions near the propeller axis), $t = r_2/r$ can be very large, leading to numerical errors in the evaluation of K, due to incorrect cancellation between large powers of t. This can be avoided by expanding in powers of $\eta = 1/t$. Writing

$$K_{2u,m+p} = \frac{1}{j2\pi} \int_{\mu_0}^{\mu_0^*} \frac{(1/\mu + \eta)^u}{(\mu + \eta)^u} \frac{\mu^{m+p}}{\mu} d\mu,$$

$$= \sum_{q=0}^{\infty} \frac{\eta^q}{q!} \frac{d^q K_{2u,m+p}}{d\eta^q}\bigg|_{\eta=0}.$$

The derivatives of $K_{2u,m+p}$ can be calculated using Leibniz' rule for differentiation of a product [30] and evaluated at $\eta = 0$, as in [16]

$$K_{2u,m+p} = -\frac{1}{\pi} \sum_{i=0}^{\infty} \binom{u+i-1}{u-1} (-\eta)^i \sum_{q=0}^{u} \binom{u}{q} \frac{\sin(2u+i-q-m-p)\theta_2^{(0)}}{2u+i-q-m-p} \eta^q. \quad (22)$$

This provides the formula necessary for the calculation of the acoustic field near the propeller axis.

4. FIELD CALCULATIONS

The acoustic field has been calculated for four sets of operating parameters. Three of these were chosen as roughly representative of real systems and the fourth was chosen to illustrate in exaggerated form some of the features of the acoustics of rotors at incidence. To allow the fields to be studied in detail, only the thickness noise term $(-jnM_t + \mathbf{M}_\infty \cdot \nabla)I$ is illustrated here. This is because its calculation requires the evaluation of all three spatial derivatives, making it a useful test of the numerical procedures, and because thickness noise is dominant in high-speed rotor acoustics, which account for three of the four cases considered. The "realistic" operating conditions chosen are a high-speed propeller in cruise ($M_t = 1{\cdot}05$, $M_\infty = 0{\cdot}8$, $\alpha = 3^\circ$), a conventional propeller at takeoff ($M_t = 0{\cdot}8$, $M_\infty = 0{\cdot}2$, $\alpha = 20^\circ$) and a helicopter rotor in forward flight ($M_t = 0{\cdot}8$, $M_\infty = 0{\cdot}2$, $\alpha = 85^\circ$). The fourth operating condition is a high-speed rotor in a low-speed mean flow ($M_t = 1$, $M_\infty = 0{\cdot}2$, $\alpha = 90^\circ$). In each case, the harmonic number $n = 16$. The operating conditions of the conventional propeller and the helicopter rotor have deliberately been made identical except for the angle of attack. This allows an assessment to be made of the acoustic effect of incidence. The last set of operating conditions was chosen to force the blade tip to oscillate about the sonic radius to examine the effect this has on the field.

The integral I was calculated over the region $-3 \leqslant z \leqslant 3$, $0 \leqslant r \leqslant 3$, with some extra points added outside this range to allow for the calculation of derivatives. The integral was evaluated at grid points spaced one-tenth of the minimum Doppler shifted wavelength apart and interpolated on to a finer mesh using cubic spline interpolation. The derivatives required for the evaluation of the acoustic field were calculated using the spline coefficients.

The acoustic field, the real part of $(-jnM_t + \mathbf{M}_\infty \cdot \nabla)I$, is shown in Figures 5–8. These figures each contain two sets of data, the first a slice through the field at $y = 0$, the second a slice at $z = 0$, across the source plane. In the first case, flow is from right to left (M_z) and bottom to top (M_x) and positive pressures are shown as solid lines, negative pressures as dashed. In the second plot of each figure, only positive pressures are shown and these are

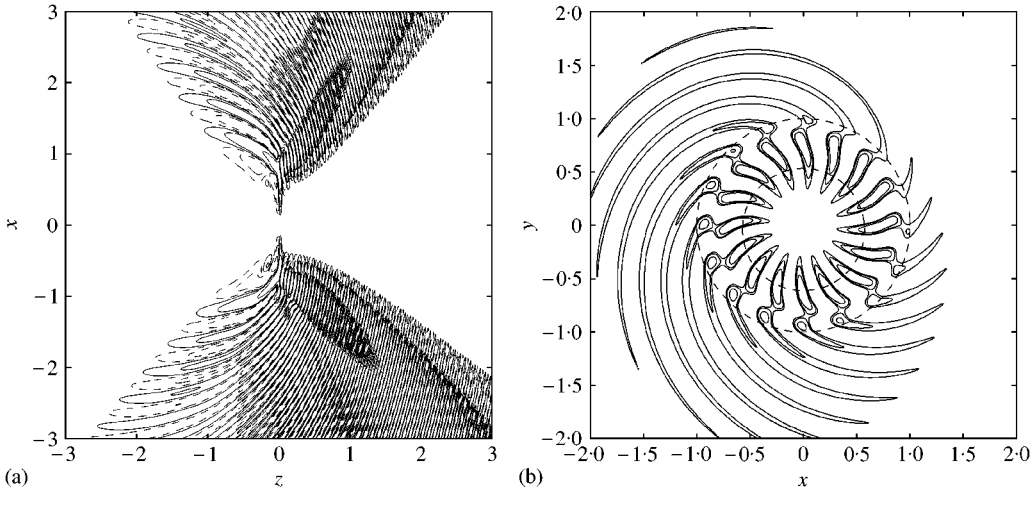

Figure 5. High-speed propeller in cruise: $M_t = 1{\cdot}05$, $M_\infty = 0{\cdot}8$, $\alpha = 3^\circ$; (a) $y = 0$, contour levels ± 1, $\pm 0{\cdot}25$, $\pm 0{\cdot}0625$; (b) $z = 0$, contour levels 2, 1, 0·5.

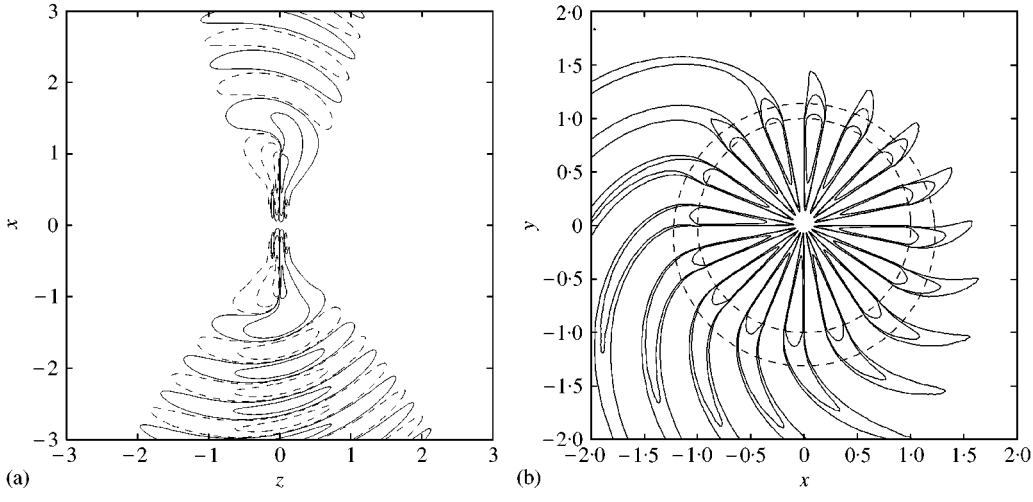

Figure 6. Conventional propeller at takeoff: $M_t = 0{\cdot}8$, $M_\infty = 0{\cdot}2$, $\alpha = 20^\circ$; (a) $y = 0$, contour levels $\pm 0{\cdot}05$, $\pm 0{\cdot}01$, $\pm 0{\cdot}001$; (b) $z = 0$, contour levels 0·1, 0·02, 0·01.

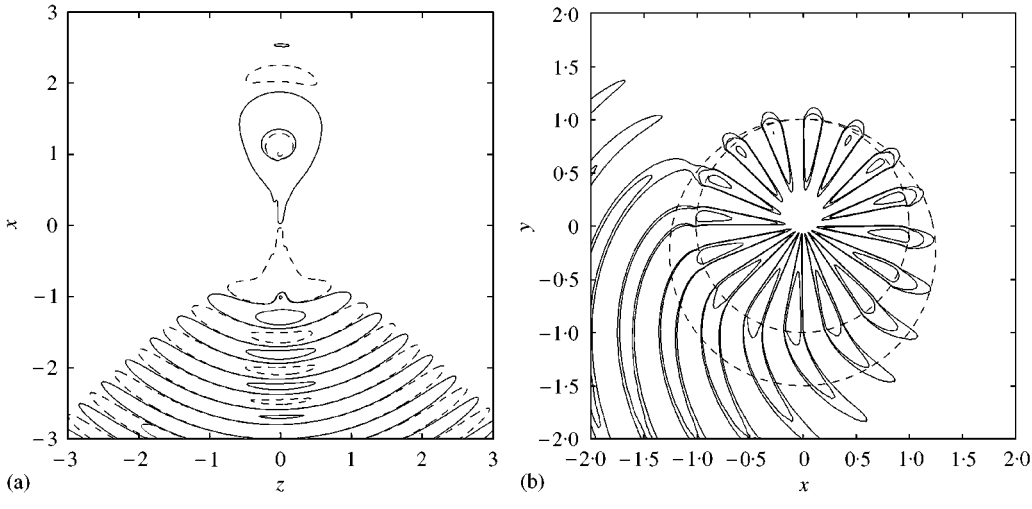

Figure 7. Helicopter rotor: $M_t = 0{\cdot}8$, $M_\infty = 0{\cdot}2$, $\alpha = 85^\circ$; (a) $y = 0$, contour levels $\pm 0{\cdot}1$, $\pm 0{\cdot}05$, $= 0{\cdot}001$; (b) $z = 0$, contour levels 0·25, 0·05, 0·025.

plotted as solid lines with the disc radius $r = 1$ and the sonic radius,

$$r^* = -\frac{M_x}{M_t}\sin\theta + \frac{(M_x^2\sin^2\theta + \beta^2)^{1/2}}{M_t}, \tag{23}$$

shown dashed.

The results shown here were spot-checked against evaluation of the two-dimensional integral of equation (5a), with the derivatives performed analytically as a check on the numerical procedures. In performing these checks, it was found that the computational effort required to evaluate the acoustic integrals using the methods of this paper was of the order of 20% of that needed for full two-dimensional integration.

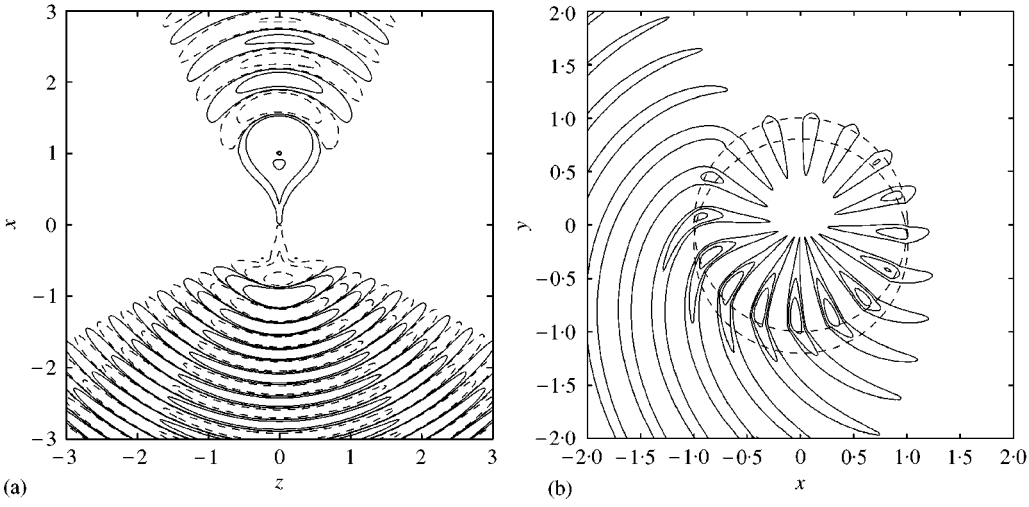

Figure 8. High-speed rotor: $M_t = 1$, $M_\infty = 0{\cdot}2$, $\alpha = 90^\circ$; (a) $\theta = 0$, contour levels $\pm 0{\cdot}1$, $\pm 0{\cdot}01$, $\pm 0{\cdot}001$; (b) $z = 0$, contour levels 1, 0·5, 0·125. The sonic radius is the lower of the two dashed curves.

4.1. HIGH SPEED PROPELLER IN CRUISE

The first set of operating conditions, Figure 5, represent a high-speed propeller ($M_t = 1{\cdot}05$) in forward flight ($M_\infty = 0{\cdot}8$) at a small angle of attack ($\alpha = 3^\circ$). While the angle of incidence is small, it gives rise to quite large effects because of the high flight speed. Figure 5(a) shows the field in the plane $y = 0$. The first point to note is the strong beaming pattern characteristic of supersonic rotors [15, 16], with sound radiated preferentially ahead of the rotor disc. There is also a strong variation in the wavelength in the far field, due to the large changes in the Doppler factor. The most obvious feature of the field, with respect to incidence, is that the main beam is much larger for negative x than for positive. This is to be expected: the source-observer Mach number is larger in the upstream M_x direction than downstream and, as explained by Hanson [23], this increase in Mach number increases the radiation efficiency of the source. Figure 5(b) shows the acoustic pressure contours in the rotor plane. The rotor disc radius and the sonic radius are also indicated to allow the application of the geometric interpretation of Chapman [15], discussed in section (2.1). Note that in this figure, the sonic radius is the innermost of the two dashed curves. As the sonic radius varies with azimuth, the rotor blades penetrate the far field by a varying amount. Since the acoustic energy from the subsonic part of the rotor has to tunnel across the transition region, the zone around the sonic radius, varying amounts of energy are lost across the transition, making the acoustic field asymmetric. Prentice [33] has shown that for a subsonic ring source, exponentially small amounts of energy leak across the transition region. If the transition region varies in thickness, even by the quite small amount of Figure 5(b), it seems reasonable that this should give rise to large variations in the acoustic energy crossing the boundary at any given azimuth, an effect made obvious in Figure 5(b). The acoustic pressure has a strong azimuthal dependence, especially in the region between the sonic and disc radii and in the far field. Naturally, the physical process at work is that described by Hanson [23], but the interpretation in terms of radiation tunnelling across the transition region is also useful.

4.2. CONVENTIONAL PROPELLER AT TAKEOFF

The next two operating conditions are identical except for their angle of attack. In Figure 6, field data are shown for a propeller of tip Mach number $M_t = 0{\cdot}8$ and a flight Mach number $M_\infty = 0{\cdot}2$ at angle of attack $\alpha = 20^\circ$, representative of a conventional propeller taking off or landing. The rotor is subsonic at all points of a revolution and the acoustic field is similar to that calculated for a subsonic rotor in earlier work [15, 16]. Figure 6(a) shows the acoustic pressure in the plane $y = 0$. There is little variation in the acoustic wavelength, due to the relatively low flight speed, and the pressure contours are bent in the direction of M_z. The far field does not display the strong beaming pattern seen in Figure 5, the side lobes being quite weak. The slice at $z = 0$ shows why. The sonic radius $r^* > 1$ at all points and the acoustic energy must tunnel across quite a wide transition region. There are variations in the thickness of this transition region, however, giving rise to asymmetry in the field. In Figure 6(a), the lobe for negative x is obviously larger than that for positive x, due to the greater source Mach number in this direction. Similarly, in Figure 6(b) radiation is clearly stronger towards the bottom left-hand corner of the plot, again due to the variation in Mach number as the source rotates.

4.3. HELICOPTER ROTOR IN FORWARD FLIGHT

The last set of realistic operating parameters is identical to that of section 4.2 but with the angle of attack increased to 85°. This makes the results representative of the acoustic field of a helicopter rotor in forward flight, as well as providing a useful comparison with the data shown in Figure 6. The combination of M_∞, M_t and α is such that the maximum tip velocity is just below sonic and the transition region thickness is almost zero at $\theta = \pi/2$. This gives rise to a very large variation in the acoustic field. Figure 7(a) shows the field at $y = 0$ and the asymmetry is quite obvious. At negative x there is a large lobe with a narrower high-pressure lobe lying inside it, almost symmetric about the source plane. On the other side of the rotor axis, the field is very weak with only a small lobe which dies away quite quickly with radius. In Figure 7(b), the reason for this strong variation is made clear. The sonic radius varies from 1·0008 to 1·50, causing large variations in the thickness of the transition region through which the acoustic energy must tunnel. In the source plane, there is a very weak acoustic field for about 180° of azimuth, with sound being radiated strongly towards the bottom left-hand corner of the plot. Again, this is a physical consequence of the variations in source-observer Mach number, but can also be quite naturally explained in the framework of the field geometry.

4.4. HIGH SPEED ROTOR AT 90° INCIDENCE

The last set of operating parameters have been chosen purely to examine the physics of the system and not for their relation to a real application. The angle of attack was set to 90° and the tip and flight Mach numbers were chosen to force the sonic radius to have values greater than and less than one. In this way, the blade tips oscillate in and out of the transition region. The operating conditions chosen were $M_x = 0{\cdot}2$ and $M_t = 1$. This leads, first of all, to an acoustic field which is symmetric about $z = 0$, as seen in Figure 8(a). The field is, not unexpectedly, much stronger upstream than downstream, i.e., for negative x. There is also a noticeable difference in the acoustic wavelength either side of the rotor axis. The source velocity downstream is greater than that upstream and this causes a marked change in the Doppler factor. Figure 8(b) showing the plane $z = 0$ demonstrates the same

effect. The variation in the thickness of the transition region, bounded by $r = 1$ and r^* is quite large and this leads to a large variation in the strength of the acoustic field, especially on the rotor disc itself. In the lower half of the disc, there are pockets of high pressure, which disappear in the upper half. As in Figure 7, the strongest radiation is in the negative x, negative y direction, where the source-observer Mach numbers are greatest.

5. CONCLUSIONS

A computationally efficient method for the exact calculation of the acoustic field of rotating sources at incidence has been developed. Results from the procedure for parameters characteristic of aircraft propellers and rotors show the structure of the acoustic field at incidence and how it is modified by the angle of attack. As shown in previous work on supersonic propellers [11, 13], the sonic radius is an essential parameter in determining the radiated acoustic field. Previous work [15] has shown that the field structure is determined by acoustic radiation tunnelling from the near field into the far field, via a transition zone around the sonic radius. In this paper, the importance of this transition has been emphasized: at incidence, the sonic radius becomes a function of angle on the rotor disc and the transition zone varies in thickness. Because the radiation decays exponentially as it crosses the transition region [33], even small variations in the sonic radius can cause large asymmetry in the far field, as seen in Figures 5–8. The observations of previous studies [20, 22, 23] have been confirmed and can now be viewed in an alternative framework which links the problem of the propeller at incidence to the asymptotic studies of supersonic rotors [11, 13] which noted the importance of the sonic radius in determining the structure of the radiated field.

REFERENCES

1. M. J. LIGHTHILL 1952 *Proceedings of the Royal Society of London A* **211**, 564–587. On sound generated aerodynamically: I. General theory.
2. J. E. FFOWCS WILLIAMS and D. L. HAWKINGS 1969 *Philosophical Transactions of the Royal Society of London A* **264**, 321–342. Sound generation by turbulence and surfaces in arbitrary motion.
3. M. GOLDSTEIN 1974 *Journal of the Acoustical Society of America* **56**, 497–509. Unified approach to aerodynamic sound generation in the presence of solid boundaries.
4. F. FARASSAT 1981 *American Institute of Aeronautics and Astronautics Journal* **19**, 1122–1130. Linear acoustic formulas for calculation of rotating blade noise.
5. F. FARASSAT 1985 in *Aerodynamics and Acoustics of Propellers*, Vol. 10. AGARD. Theoretical analysis of linearized acoustics and aerodynamics of advanced supersonic propellers.
6. D. B. HANSON 1983 *American Institute of Aeronautics and Astronautics Journal* **21**, 881–888. Compressible helicoidal surface theory for propeller aerodynamics and noise.
7. LYLE N. LONG and KENNETH S. BRENTNER 2000 in 38*th Aerospace Sciences Meeting and Exhibit*. New York: AIAA. Self-scheduling parallel methods for multiple serial codes with application to WOPWOP.
8. E. J. H. LYNAM and H. A. WEBB 1919 *Reports and Memoranda* 624 *Aeronautical Research Committee*. The emission of sound by airscrews.
9. L. GUTIN 1948 *Technical Memorandum* 1195 *NACA*. On the sound field of a rotating propeller.
10. I. E. GARRICK and C. E. WATKINS 1953 *Report* 1198 *NACA*. A theoretical study of the effect of forward speed on the free-space sound-pressure field around propellers.
11. N. PEAKE and D. G. CRIGHTON 1991 *Journal of Fluid Mechanics* **232**, 285–301. An asymptotic theory of near-field propeller acoustics.
12. A. B. PARRY and D. G. CRIGHTON 1989 *American Institute of Aeronautics and Astronautics Journal* **27**, 1184–1190. Asymptotic theory of propeller noise. Part I: subsonic single rotation propeller.

13. D. G. CRIGHTON and A. B. PARRY 1991 *American Institute of Aeronautics and Astronautics Journal* **29**, 2031–2037. Asymptotic theory of propeller noise. Part II: supersonic single rotation propeller.
14. C. J. CHAPMAN 1990 *Proceedings of the Royal Society of London A* **431**, 157–167. The spiral Green function in acoustics and electromagnetism.
15. C. J. CHAPMAN 1993 *Proceedings of the Royal Society of London A* **440**, 257–271. The structure of rotating sound fields.
16. M. CARLEY 1999 *Journal of Sound and Vibration* **225**, 353–374. Sound radiation from propellers in forward flight. doi:10.1006/jsvi.1999.2284.
17. M. CARLEY 2000 *Journal of Sound and Vibration* **233**, 255–277. Propeller noise fields. doi:10.1006/jsvi.1999.2797
18. S. E. WRIGHT 1969 *Journal of Sound and Vibration* **9**, 223–240. Sound radiation from a lifting rotor generated by asymmetric disk loading.
19. R. STUFF 1988 *American Institute of Aeronautics and Astronautics Journal* **26**, 777–782. Noise field of a propeller with angular inflow.
20. R. MANI 1990 *Proceedings of the Royal Society of London A* 431, 203–218. The radiation of sound from a propeller at angle of attack.
21. D. B. HANSON and D. J. PARYZCH 1993 *NASA Contractor's Report* 4499 *Hamilton Standard Division, United Technologies Corporation, P.O. Box* 100, *Windsor Locks, Ct* 06096, *U.S.A.* Theory for noise of propellers in angular inflow with parametric studies and experimental verification.
22. E. ENVIA 1993 in *Proceedings of the Sixth International Symposium on Unsteady Aerodynamics, Aeroacoustics and Aeroelasticity of Turbomachines and Propellers*, 685–703. Berlin: Springer-Verlag. Prediction of noise field of a propfan at angle of attack.
23. D. B. HANSON 1995 *Proceedings of the Royal Society of London A* **449**, 315–328. Sound from a propeller at angle of attack: a new theoretical viewpoint.
24. M. V. LOWSON 1965 *Proceedings of the Royal Society of London A* **286**, 559–572. The sound field for singularities in motion.
25. M. Carley 1996 *Ph.D. Thesis, Trinity College, Dublin* 2, *Ireland*. Time domain calculation of noise generated by a propeller in a flow.
26. F. FARASSAT, M. H. DUNN and P. L. SPENCE 1992 *American Institute of Aeronautics and Astronautics Journal* **30**, 2337–2340. Advanced propeller noise prediction in the time domain.
27. D. B. HANSON 1992 *American Institute of Aeronautics and Astronautics Journal* **30**, 2334–2337. Direct frequency domain calculations of open rotor noise.
28. A. D. Pierce 1989 *Acoustics: An Introduction to its Physical Principles and Applications*. Acoustical Society of America, New York.
29. G. N. WATSON 1995 *A Treatise on the Theory of Bessel Functions*. Cambridge: Cambridge University Press.
30. I. GRADSHTEYN and I. M. RYZHIK 1980 *Table of Integrals, Series and Products*. New York: Academic Press; 5th edition.
31. M. VAN DYKE 1984 *Annual Review of Fluid Mechanics* **16**, 287–309. Computer-extended series.
32. E. KREYSZIG 1993 *Advanced Engineering Mathematics*. New York: Wiley.
33. P. R. PRENTICE 1993 *Proceedings of the Royal Society of London A* **441**, 83–96. Energy transport in rotating sound fields.